Bio-Medical Materials and Engineering 24 (2014) 3471–3478
DOI 10.3233/BME-141172
IOS Press

Quantification of osteoarticular joint defects through bone segmentation and modeling

Jian Yang[a], Tianyu Fu[b], Danni Ai[a], Huijun Xing[b], Qin Li[b,*] and Yongtian Wang[a]
[a]*Beijing Engineering Research Center of Mixed Reality and Advanced Display, School of Optics and Electronics, Beijing Institute of Technology, Beijing 100081, China*
[b]*School of Life Science, Beijing Institute of Technology, Beijing 100081, China*

Abstract. Shoulder instability is a major threat to people's daily life. Many patients suffer from shoulder instability such as the loss of the glenoid and humeral head. In clinical practice, an accurate 3D structure estimation of damaged joints is necessary to diagnose and treat bone defects. This study quantifies osteoarticular defects through the modeling and visualization of osteoarticular structures. An improved algorithm to extract the 3D structure of the bones is proposed. The bone contour is then automatically extracted using prior shape and gray scale intensity distribution of joint CT images. Joint structures with mirror symmetry are matched using the Iterative Closest Point registration algorithm. Osteoarticular defects can be quantified on the basis of the symmetric information of the bones. Experimental results demonstrate that the proposed method can effectively segment the joint structures from the CT image. In addition, the proposed mirror symmetrical method can effectively estimate osteoarticular defects.

Keywords: Joint bone, segmentation, modeling, quantitative analysis

1. Introduction

Daily exercise is closely related to the joints of the human body. Joint defects may seriously affect people's daily activities. In osteoarthropathy, the anterior dislocation of the shoulder joint is a common orthopedic disease. Clinical statistics show that approximately 90% of anterior shoulder dislocation cases result from osseous tissue defects [1]. Joint replacement is an effective approach for joint defect treatment. However, different people usually have various bone shapes and sizes. Hence, prosthetic joints do not usually match the bones to resume their normal physiological functions. Personalized joint arthroplasty as a method to assist the diagnosis and treatment of joint defects has attracted considerable attention [2,3]. This method is used to design individualized artificial prosthesis based on the patient's CT or MRI images. Hence, personalized prosthesis may, in the largest extent, match with the anatomical structure of the patient's lesions. Quantifying bone defects from CT or MRI images is crucial for bone transplantation.

Successful joint defect treatment is limited by the lack of a precise joint model and personalized treatment. However, modeling and visualization technologies based on medical imaging can provide

*Corresponding author: Qin Li, School of Life Science, Beijing Institute of Technology, Beijing 100081, China. Tel.: 8610 6891 5998; Fax: 8610 6891 5956; E-mail: liqin@bit.edu.cn.

physicians with the stereoscopic structure and quantified defecting parameters of the joints, from which physicians can diagnose and treat joint defects quickly and accurately. For such technology, accurate extraction and modeling of the joint structure are important to quantify joint defects from geometric parameters. Given its high individuation, image-guided bone joint quantification is valuable in clinical practice [4,5].

Recent studies have extensively investigated the segmentation and modeling of joint structures. Chung et al. [4] used the adaptive threshold method to detect bone boundaries, which are then utilized to control the scope of the region growing method. For this method, the proposed adaptive region growing method has a strong anti-noise mechanism to achieve the accurate segmentation of bone structures. However, this approach is effective only when the gray level distributions are non-uniformly connected with the extracting targets. For bone structures with weak boundaries, the method is prone to leaks and leads to adjacent soft tissues. Lee et al. [6,7] used the graph cut method to calculate the optimal value of the energy equation based on Markov's model and then extracted the knee joint structure. However, this method is time consuming [8].

Basing on previous studies, this study proposes a novel method for the modeling and visualization of joints to address the problems mentioned above. Shape and intensity data are combined as the prior conditions for the level set calculation. Then, the mirror symmetrical feature of the joints of the left and right shoulders of the human body is utilized to estimate the defect of one side by the other side. The joints on the left and right shoulders are matched using the point cloud registration method. Thereafter, the segmented joint structure is utilized to quantify the osteoarticular defects.

2. Method

This study proposes a novel method to model and visualize osteoarticular defects. Basing on the level set energy function proposed by Li et al. [9], the prior shape information and intensity information are integrated for joint segmentation. After the bone structures of the left and right shoulders are extracted, the Iterative Closest Point (ICP) method is used to register the structures together. Hence, the geometric distribution of the defect structure can be effectively quantified.

2.1. Prior information of shape

The target of bone segmentation is to extract the outline of the bone structures. Generally, the intensity distributions of the cortex and marrow are different, and the intensity distribution of the marrow is very close to that of the background. Therefore, this study proposes to use the level set method for joint segmentation. Initial contour larger than the cortex of the joint is delineated manually in a selected cross-section [10], which is formulated by a symbolic distance function. The internal and external points for this function are negative and positive, respectively. Then, the level set algorithm is used for curve evolution in the cross-section, and the results are set as the initial contour for the lower and upper cross-sections. The difference between the contours of the two adjacent cross-sections is small; hence, the obtained initial contour is accurate enough to enclose the bone structures in the cross-section.

Moreover, the gray-scale distributions inside the bone structures are considerably uneven while the distributions for the adjacent bone structures are highly similar because of the different absorption rates of the cortex and the marrow. Hence, the shape information of the bones in the predefined cross-section can be utilized as a reference to determine the adjacent boundaries. Furthermore, the reference

shape can be utilized as the stop function of the level set algorithm. For the level set function ϕ, the gradient $\nabla\phi(x,y)$ of a point (x,y) in the image can be defined as follows:

$$\nabla\phi(x,y)=\left[\frac{\phi(x+1,y)-\phi(x-1,y)}{2},\frac{\phi(x,y+1)-\phi(x,y-1)}{2}\right] \tag{1}$$

The gradient vectors of the level set function are illustrated in Figure 1. Results show that the boundaries are rested at the edges with different directions of level set gradient and image gradient. Hence, the stop function g can be defined as follows:

$$g=\begin{cases}\dfrac{1}{1+(|\nabla I|/K)^2}, \nabla\phi\cdot\nabla I<0\\ 1, \nabla\phi\cdot\nabla I\geq 0\end{cases} \tag{2}$$

where ∇I represents the gradient of image and K is a constant with a value greater than one. When the directions of the level set function and the image gradient are opposite each other, the inner boundary should be captured (Figure 1(a)). In such cases, the stop function of the level set must be changed in such a way that the iteration can proceed and reach the true outer boundary. By contrast, when the directions of the level set function and image gradient are identical, the target boundary should be captured (Figure 1(b)).

Generally, the image gradient is comparatively small for pixels inside the target. We have $|\nabla I|<K$, and the value of g is large. For such cases, the level set iteration will continue. By contrast, for pixels near the boundary, the absolute value of the gradient is greater than K, the value of g is small, and the iteration will slow down and finally approach the boundary of the target. Furthermore, greater K means fewer boundary details can be obtained. Hence, the detected edges with large gradient values will be regarded as the boundary, whereas the edges with small gradient values will be classified as the background.

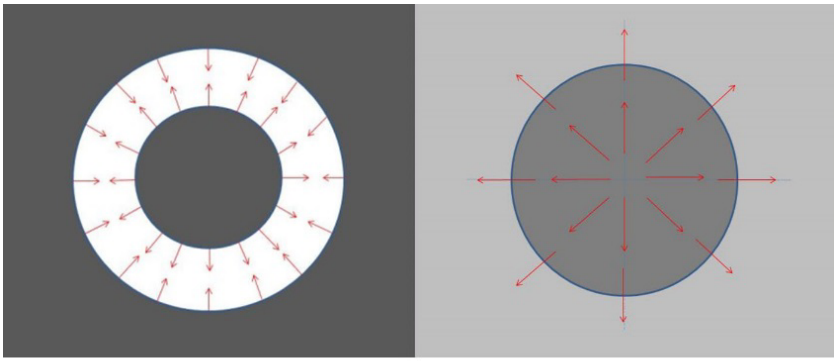

Fig. 1. Schematic diagram of gradient calculation. (a) The direction vectors of gradient for image with inner boundary. (b) The direction vectors of the gradient for the level set function.

2.2. Prior information of intensity

For image areas with weak boundaries, accurately segmenting the boundaries by merely calculating the image gradient is difficult. Hence, this study introduces the image difference between adjacent cross-sections for accurate boundary extraction. Let $P_T(I(x,y))$ and $P_B(I(x,y))$ represent the probabilities of a pixel (x,y) belonging to segmenting target and background, and let $I(x,y)$ represent the pixel intensity. Therefore, the energy equation can be defined as follows:

$$\varepsilon(\phi)=\mu\int_\Omega p(|\nabla\phi|)dxdy+\lambda\int_\Omega g\delta(\phi)|\nabla\phi|dxdy+\nu\int_\Omega f(I_0)gH(-\phi)dxdy \tag{3}$$

$$f(I(\mathrm{x},\mathrm{y}))=\begin{cases}v'[P_B(I(x,y))-P_T(I(x,y))] & P_B(I(x,y))-P_T(I(x,y))\neq 0\\ 1 & P_B(I(x,y))-P_T(I(x,y))=0\end{cases} \tag{4}$$

where $H(\cdot)$ is the unit step function, $\delta(\cdot)$ is the Dirac function, $p(\phi)=\int_\Omega\frac{1}{2}(|\nabla\phi|-1)^2dxdy$ .While μ , λ and ν are the weighting coefficients. The first and second terms in Eq. (3) are similar to the terms defined by Li [9], whereas the third term is defined to utilize the prior information of intensity distribution. P_B and P_T are calculated by the segmentation results of the adjacent cross-sections. The difference between P_B and P_T clearly decides the evolution direction of the initialized contour. Moreover, a small difference between P_B and P_T indicates that the segmentation results will be similar to that of the former cross-section; hence, the evolution direction of the contour will follow the principle of the former cross-section. If P_B is greater than P_T , then the value of $f(I_0)$ is positive. This condition indicates that the contour is in the image background. By contrast, if P_T is greater than P_B , then the value of $f(I_0)$ is negative. This condition indicates that the contour is in the foreground region of the image. The prior information of the former cross-section defines the initial contour of the current cross-section, and the defined prior gray information determines the contour contracting. To minimize the above defined energy function, the evolution of the level set can be calculated as follows:

$$\frac{\partial\phi}{\partial t}=\mu div(d_p(|\nabla\phi|)\nabla\phi)+\lambda\delta(\phi)div(g\frac{\nabla\phi}{|\nabla\phi|})+\nu f(I_0)g\delta(\phi) \tag{5}$$

where $div(\cdot)$ is the divergence function.

The probabilities of the target and background are calculated in a narrow band of the image; hence, we only need to calculate the histogram distribution of the former cross-section in a narrow predefined area. In this manner, the calculation efficiency can be significantly improved. This study simplifies the probability calculation method proposed by Gao et al. [11] and allows the deforming contour to shrink or expand adaptively. The use of prior shape information can accurately provide an initial contour for the current cross-section, whereas the use of prior intensity information can estimate the evolving direction of the contour in a narrow band from the former cross-section. In addition, the deformation size is determined by the coefficient. In other relevant topological shape methods, a large shrinkage

coefficient is typically required. Therefore, a large expansion coefficient means the contour is likely to expand into the boundaries of the surrounding bones.

2.3. Defect quantification

By the above segmentation method, the joint structures of the left and right shoulders can be obtained. The bone structures of the left and right shoulders show mirror symmetry; hence, the bone structure of the shoulder without damage can be utilized as the base to quantify the degree of defect of the other shoulder. In this study, the defect ratio is utilized to quantify the defect degree of the osteoarticular joint. The defect ratio is defined as the volume of damaged bone structure in relation to the total volume of bone structure. The defect ratio of the osteoarticular joint is quantified by performing mirror transformation of the segmented model of the normal joints and then introducing the ICP registration method for the registration of the mirror-transformed bone structure to the damaged joints. The target of the point cloud registration is to find the best transformation between the source and target point clouds that leads to the minimum Euclidian distance between the closest points between the two point clouds.

Let $\{P_i \mid P_i \in R^3,\ i=1,2,\cdots,m\}$ and $\{P_j \mid P_j \in R^3,\ j=1,2,\cdots,n\}$ represent the vertices of the segmented bone structure meshes of the normal and damaged bone joints, where m and n represent the number of vertices. The aim of the registration process is to minimize the following target function:

$$e^2(R,t) = \min \sum_{1}^{n} \| Q_i - (\mathrm{s}\cdot R \cdot P_i + t) \|^2 \tag{6}$$

where R and t represent the 3×3 transformation matrix and 3×1 translation vector, respectively, and s is the scaling factor between the normal and abnormal bone structures.

The joint sizes are usually unequal when the point clouds of the left and right joints of the same person are registered. This finding is reasonable because the developments of the joints on the left and right sides of different people are determined by different factors, such as genes and habits. Therefore, the scaling ratio s of the normal and abnormal joints must be used to quantify the defect ratio of the damaged joints relative to the normal joints. Once the bone structures of the left and right shoulders are registered together and the scaling coefficient is determined, the difference between the structures can be effectively quantified. Furthermore, the defect ratio can be calculated as follows:

$$D = \left| \mathrm{s}\cdot V_{normal} - V_{abnormal} \right| / (\mathrm{s}\cdot V_{normal}) \tag{7}$$

where V_{normal} and $V_{abnormal}$ represent the segmented volumes of normal and abnormal joints, respectively.

3. Experiment

To validate the performance of the proposed method, a series of experiments is designed using the CT images of the left and right shoulders. The data sets used for the experiments are obtained from the Peking University Third Hospital, Beijing. All data sets have the resolution size of $512\times512\times120$,

and 20 groups of CT data are utilized for the experiments. The entire algorithm is implemented in the C++ programming language in the Linux platform, and the experiments are performed on a relatively low-cost desktop computer with an i7-2600 processor and 16 G memory.

Figure 2 shows the segmentation results of the traditional level set method (a and c) and the proposed method (b and d). Results show that the traditional method is not efficient to segment bone structures in the CT image and that the segmentation may fail in the areas with closed boundaries or inhomogeneous density distribution. By contrast, the proposed method accurately segments the bone structures from the CT image, which shows that the contour accurately evolves toward the bone outline. Therefore, the proposed method clearly outperforms the traditional level set method.

Figure 3 shows the segmentation results of six cross-sections of the joints in the CT images using the proposed method. In this figure, (a), (b), and (c) are the 30^{th}, 50^{th}, and 70^{th} cross-sections of a normal joint, whereas (d), (e), and (f) are the 20^{th}, 60^{th}, and 70^{th} cross-sections of a damaged joint. The

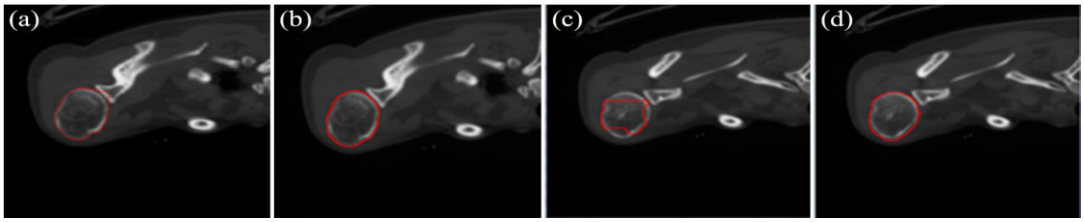

Fig. 2. Experiments of traditional level set and the proposed methods. (a) and (c) are the segmentation results of the level set method in two different cross-sections. (b) and (d) are the segmentation results of the proposed method corresponding to the cross-sections of (a) and (c), respectively.

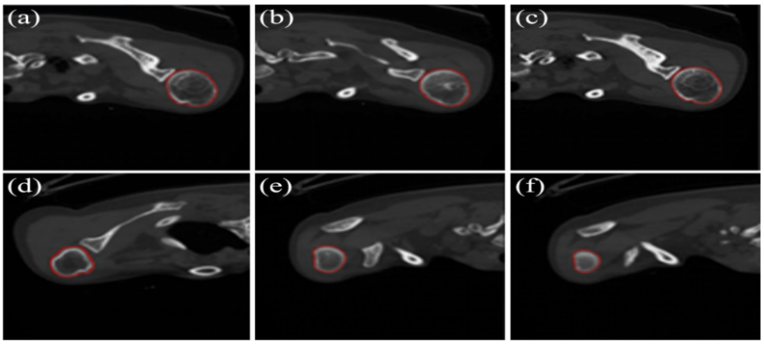

Fig. 3. Segmentation results of six cross-sections of the joint bone in the CT image by the proposed method. (a), (b) and (c) are 30^{th}, 50^{th} and 70^{th} cross-sections of a normal joint; while (d), (e) and (f) are 20^{th}, 60^{th} and 70^{th} cross-sections of a diseased joint.

Table 1

Quantification of the calculation results on three data sets

	V_{normal} (cm^3)	$V_{abnormal}$ (cm^3)	Scaling Ratio	Defect Ratio
Data 1	546.19	553.86	1.05	3.8%
Data 2	543.72	550.97	1.09	8.4%
Data 3	406.08	552.81	1.12	6.4%

segmentation results show that the proposed method can accurately segment both normal and damaged bone structures from the CT images. The figures also show that parts of the bone structures are close to the neighboring bones in (a), (b), (c), and (d). Moreover, the proposed method can effectively delineate the boundaries of the interesting bone structures from the background and other bone structures. In addition, the marrow inside the bone structures takes large areas in (a) and (c), and its gray intensity is slightly inhomogeneous. Nevertheless, the proposed method can still accurately segment the outline of the bone structures.

Table 1 demonstrates the defect quantification results of three randomly selected data sets. Data 1 shows that the volumes of normal and abnormal joints are 546.19 and 553.86 cm^3, respectively. The scaling ratio is 1.05, and the calculated defect ratio is 3.8%. Data 2 shows that the volumes of normal and abnormal joints are 543.72 and 550.97 cm^3, respectively. The scaling ratio is 1.09, and the calculated defect ratio is 8.4%. Data 3 shows that the volumes of normal and abnormal joints are 406.08 and 552.81 cm^3, respectively. The scaling ratio is 1.12, and the calculated defect ratio is 6.4%. For all the three data sets, the sizes of the abnormal joints are greater than those of the normal joints. Despite this difference, the proposed method can effectively quantify the defect ratio of the abnormal joints.

Figure 4 shows the registration results of the normal and abnormal joints in 3D space. In the figure, (a) shows the rendering result of the registered point clouds, and (b) shows the rendering of the registered meshes of the bone structures. In addition, the red points and mesh represent the data sets of the abnormal joints, and the green data sets are those of the normal joints. The two data sets are effectively registered together, and the difference between these two data sets can be visually compared.

4. Conclusion

This study proposes a novel method to quantify osteoarticular defects using CT images of the left and right shoulders of the patient. A novel level set based method is proposed to segment interesting joint structures. To improve the accuracy of segmentation, the prior data on the intensity distribution and shape of the bone structure of neighboring cross-sections of the CT image are combined into the level set framework. The outlines of the joint structures have already been delineated from the background; thus, the provided shape and intensity distributions in the neighboring cross-section can

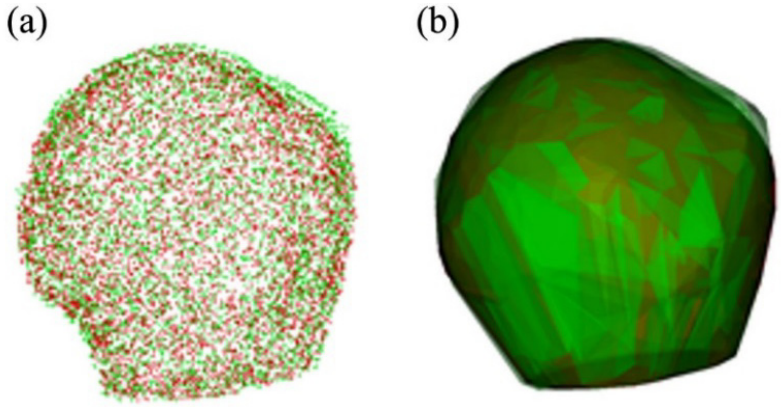

Fig. 4. Result of the point cloud registration. (a) and (b) are the rendering of the registered point clouds and the meshes of the bone structures.

effectively drive the deforming contour to approach the segmentation target. To quantify the defect structure of the joint, the ICP algorithm is introduced to register the normal and abnormal joint structures. The scaling factor between the normal and abnormal joint structures can also be estimated during registration. Thereafter, the defect ratio of the abnormal joints can be effectively quantified by calculating the topological difference between the two registered joint structures. Experimental results demonstrate that the proposed segmentation and registration techniques are effective to quantify the joint structures.

The proposed method utilizes the mirror symmetry of the left and right joints to quantify the damaged structures of the abnormal joints. Hence, this method is not appropriate for people with abnormal joints on both left and right shoulders. Therefore, future research should focus on non-rigid registration techniques for quantifying largely deformed bone structures.

Acknowledgement

This work was supported by the National Basic Research Program of China (2010CB732505, 2013CB328806), the Key Projects in the National Science & Technology Pillar Program (2013BAI01B01), the National Hi-Tech Research and Development Program (2013AA013703).

References

[1] M.J. DiPaola, L.M. Jazrawi, A.S. Rokito, Y.W. Kwon, L. Patel, B. Pahk and J.D. Zuckerman, Management of humeral and glenoid bone loss associated with glenohumeral instability, Bull NYU Hosp. Jt. Dis. **4** (2010), 245–250.

[2] R.H. Choplin, C.N. Henley, E.M. Edds, W. Capello, J.L. Rankin and K.A. Buckwalt er, Total hip arthroplasty in patients with bone deficiency of the acetabulum, Radiographics **3** (2008), 771–786.

[3] J. Correia, D. Kendoff, T.O. Klatte, T. Gehrke and M. Citak, Percutaneous cementation: A case of a failed treatment of a loose revision total knee arthroplasty, Technol. Health Care **4** (2014), 1–6.

[4] M.A. Rerko, X.L. Pan, C. Donaldson, G.L. Jones and J.Y. Bishop, Comparison of various imaging techniques to quantify glenoid bone loss in shoulder instability, Journal of Shoulder and Elbow Surgery **4** (2013), 528–534.

[5] K.S. Kim, Y.M. Kang, J.Y. Lee, E.S. Kim, C.H. Kim, B.H. Min, H.B. Lee, J.H. Kim and M.S. Kim, Injectable cmc/pei gel as an in vivo scaffold for demineralized bone matrix, Bio-Medical Materials and Engineering **6** (2009), 381–390.

[6] C.Y. Huang, L.J. Luo, P.Y. Lee, J.Y. Lai, W.T. Wang and S.C. Lin, Efficient segmentation algorithm for 3d bone models construction on medical images, Journal of Medical and Biological Engineering **6** (2011), 375–386.

[7] S. Lee, S.H. Park, H. Shim, I.D. Yun and S.U. Lee, Optimization of local shape and appearance probabilities for segmentation of knee cartilage in 3-d MR images, Computer Vision and Image Understanding **12** (2011), 1710–1720.

[8] M.S. Aslan, A. Ali, H. Rara, B. Arnold, A.A. Farag, R. Fahmi and P. Xiang, A novel 3d segmentation of vertebral bones from volumetric CT images using graph cuts, Pt. 2 Proceedings of Advances in Visual Computing **5876** (2009), 519–528.

[9] C.M. Li, C.Y. Xu, C. Gui and M.D. Fox, Level set evolution without re-initialization: A new variational formulation, Proceedings of 2005 IEEE Computer Society Conference on Computer Vision and Pattern Recognition **1** (2005), 430–436.

[10] C.M. Li, C.Y. Xu, C.F. Gui and M.D. Fox, Distance regularized level set evolution and its application to image segmentation, IEEE Transactions on Image Processing **1** (2011), 299–299.

[11] H. Gao and O. Chae, Individual tooth segmentation from CT images using level set method with shape and intensity prior, Pattern Recognition **7** (2010), 2406–2417.